Article ID: 1000-7032(2022)07-1102-12

Achieving Efficient Violet-blue Organic Light Emitting Devices (CIE_y=0.046) by Extending π-conjugation in D-π-A Structure

CUI Jiang-feng[1], SUN Jing[1,2*], WANG Guo-liang[1], WANG Zhi-heng[1], YANG Xiao-dong[1], XU Hui-xia[1], MIAO Yan-qin[1,2], WANG Long[1], YU Jun-sheng[3], WANG Hua[1*]

(1. *Key Laboratory of Interface Science and Engineering in Advanced Materials, Ministry of Education, Taiyuan University of Technology, Taiyuan* 030024, *China*;
2. *Shanxi-Zheda Institute of Advanced Materials and Chemical Engineering, Taiyuan* 030024, *China*;
3. *State Key Laboratory of Electronic Thin Films and Integrated Devices, School of Optoelectronic Information, University of Electronic Science and Technology of China, Chengdu* 610054, *China*)
* *Corresponding Authors, E-mail: sunjing@tyut. edu. cn; wanghua*001*@tyut. edu. cn*

Abstract: Organic violet-blue luminescent materials have exhibited great potential in full-color displaying and lighting fields. However, it is a huge challenge to develop efficient violet-blue emitters because of the inherently wide energy gap. In this work, two violet-blue emitters with donor (D)-π-acceptor (A) type using 10H-phenothiazine 5,5-dioxide (2OPTZ) as a weak acceptor and N-(2-naphthyl) aniline (PNA) as the donor, namely 2OPTZ-PNA and 2OPTZ-BP-PNA, were designed and synthesized. By extending π-conjugation length between donor and acceptor, local excited states and charge transfer excited states were adjusted, and absolute photoluminescence quantum yields (PLQYs) values in the evaporated film increased from 14% to 33%. Notably, non-doped device based 2OPTZ-BP-PNA exhibits violet-blue light at 436 nm with a narrow full width at half-maximum (FWHM) of 54 nm, Commission Internationale de l'Eclairage (CIE) coordinates of (0. 155, 0. 046) and external quantum efficiency (EQE) of 4. 1%. Given this, our results provide an efficient design strategy for the high-quality violet-blue luminescent materials.

Key words: organic light-emitting diodes(OLED); violet-blue; phenothiazine dioxide; D-π-A structure; π-conjugation length
CLC number: TN312. 8 **Document code**: A **DOI**: 10. 37188/CJL. 20220093

通过拓展 D-π-A 结构中的 π 桥实现高效紫蓝光有机发光器件(CIE_y=0.046)

崔江峰[1], 孙 静[1,2*], 王国良[1], 王智恒[1], 杨晓东[1], 许慧侠[1], 苗艳勤[1,2], 王 龙[1], 于军胜[3], 王 华[1*]

(1. 太原理工大学 新材料界面科学与工程教育部重点实验室, 山西 太原 030024;
2. 山西-浙大先进材料与化学工程研究所, 山西 太原 030024;
3. 电子科技大学光电信息学院 电子薄膜与集成器件国家重点实验室, 四川 成都 610054)

摘要: 紫蓝光有机发光材料在全彩显示和照明领域具有广阔的应用前景。但是该类材料需要宽能隙,因此开

收稿日期: 2022-03-18; **修订日期**: 2022-04-05
基金项目: 国家自然科学基金(62074109,6207031407); 山西省自然科学基金(201901D211090,201901D111108); 国家自然科学基金联合基金(U21A20492); 山西省留学基金项目(2020-049)资助
Supported by National Natural Science Foundation of China(62074109,6207031407); Shanxi Province Natural Science Foundation(201901D211090,201901D111108); The Joint Funds of the National NSFC(U21A20492); Research Project Supported by Shanxi Scholarship Council of China(2020-049)

发高效的紫蓝色材料是一项巨大的挑战。本文利用10H-吩噻嗪5,5-二氧化物(2OPTZ)作为弱受体、N-苯基-2-萘胺(PNA)作为供体,设计合成了两个具有D-π-A型结构的紫蓝色材料,命名为2OPTZ-PNA和2OPTZ-BP-PNA。通过延长给受体之间的π共轭长度,使局域态和电荷转移态被优化,并且薄膜中的绝对量子产率从14%提高到33%。此外,利用2OPTZ-BP-PNA制备的非掺杂器件呈现紫蓝光(436 nm)发射,半峰全宽为54 nm,色坐标为(0.155,0.046),外量子效率为4.1%。鉴于此,本文提供了一种制备高质量紫蓝发光材料的有效策略。

关　键　词: 有机发光二极管; 紫蓝色; 二氧化吩噻嗪; D-π-A结构; π共轭长度

1　Introduction

Organic light-emitting diodes(OLEDs) play an essential role in full-color flat-panel displaying and lighting fields due to high color contrast, low driving voltages, fast response and environmental friendliness[1-6]. High-efficiency violet-blue emitters are significant to OLEDs because they can not only be employed as energy donors to generate light covering the entire visible light region, but also reduce power consumption[7-10]. In addition, the violet-blue light-emitting materials are also widely used in phototherapy[11], biological and chemical sensing[12-13], high-density information storage[14], sterilization and so on[15]. Therefore, developing high-performance violet-blue light-emitting materials is an integral part of the OLEDs technology field[16-19].

In principle, excellent violet-blue emitters require wide optical band gaps, rigid planar structures, conjugated backbones, and the ability to balance electron and hole transport[20-23]. Recently, violet-blue emitters with D-π-A structure were reported by using weak electron donors and acceptors[24-26]. On this basis, reasonable regulation of the intramolecular charge transfer (ICT) state is the key to achieve violet-blue emitter, which satisfies the color standards of violet-blue light with CIE coordinates(x, y)=(0.131, 0.046), defined by the ITU-R Recommendation BT. 2020[27-29].

It is known that phenothiazine has excellent electron donating ability and was widely used in the D-π-A system for high-performance electroluminescent materials[30-31]. Interestingly, 10H-phenothiazine 5,5-dioxide exhibits weaker electron-donating ability than phenothiazine and is widely used to construct room temperature phosphorescent materials[32-33]. In 2021, Prof. Rout *et al.* reported the influence of the oxidation state of the sulfur atom in phenothiazine on the photophysical and electrochemical properties of the compound. The results show that the oxygen-functionalized molecular structure is more rigid, the absorption and emission spectra are blue-shifted, and the highest occupied molecular orbital (HOMO) energy level is deeper[34]. In addition, it is also verified that the oxidized oxygen-functionalized molecules possess better thermal stabilities and significantly lower the lowest unoccupied molecular orbital (LUMO) energy levels, which endows better electron-injection and transport abilities[35]. In 2016, Prof. Ma and his co-workers designed and synthesized a series of triphenylamine-phenirimidazole derivatives. By gradually adding phenyls along with horizontal and vertical directions, respectively, the appropriate composition between the locally-excited (LE) state and the charge-transfer (CT) state components were adjusted and controlled, thereby effective electroluminescence(EL) efficiency was achieved[36-37].

In this work, we designed and synthesized two new D-π-A-typed violet-blue fluorescent emitters using 10H-phenothiazine 5,5-dioxide (2OPTZ) as the weaken acceptor and N-(2-naphthyl) aniline (PNA) as the donor, namely 2OPTZ-PNA and 2OPTZ-BP-PNA. By extending the length of the π-bridge between the donor and acceptor, the local excited and charge transfer states were optimized, and their absolute PLQYs values increased from 14% to 33%. Non-doped devices of 2OPTZ-PNA and 2OPTZ-BP-PNA exhibited violet-blue emission with the CIE coordinates of (0.164, 0.060) and (0.155, 0.046), respectively, maximum external quantum efficiency(EQE) of 1.5% and 4.1%, respectively, which indicated the excellent application prospect of 10H-phenothiazine

5,5-dioxide in the violet-blue OLED materials.

2 Experiment

2.1 Synthesis

The synthetic routes of 2OPTZ-PNA and 2OPTZ-BP-PNA are shown in Fig. 1, and the intermediates and target products were prepared by palladium-catalyzed Ullmann reaction and then purified by silica gel column chromatography[38-40]. Their precise structures were characterized by ^{1}H-NMR spectra, ^{13}C-NMR spectra and high-resolution mass spectrometry (Fig. S1-S3).

2.1.1 2OPTZ-PNA

Synthesis of 1a. The materials of 10H-phenothiazine (1.99 g, 10 mmol), 1-bromo-4-iodobenzene (5.66 g, 20 mmol), tri-tert-butylphosphine tetrafluoroborate (0.17 g, 0.60 mmol), sodium tert-butoxide (1.92 g, 20 mmol), tris(dibenzylideneacetone)dipalladium (0.28 g, 0.30 mmol) were dissolved in toluene (50 mL). The mixture solution was heated to 110 ℃ and reacted for 8 h. When the reaction was completed, the reaction solution was extracted, dried and subjected to column chromatography to obtain a white solid (2.15 g, yield 61%). ^{1}H NMR (600 MHz, chloroform-d): δ=8.17(dt, J=8.0, 1.7 Hz, 2H), 7.85-7.83(m, 2H), 7.41(ddd, J=8.7, 7.2, 1.6 Hz, 2H), 7.30-7.26(m, 4H), 6.62(dd, J=8.7, 0.9 Hz, 2H).

Synthesis of 2a. The intermediate of 1a(1.20 g, 3.40 mmol) was dissolved in 40 mL dichloromethane and stirred. Glacial acetic acid(20 mL) and aqueous hydrogen peroxide solution(8 mL, 30%) were added to the reaction mixture, and then the mixture was heated to 70 ℃ for 8 h. When the reaction was over, the reaction solution was extracted, dried and column chromatography to give a white solid (1.18 g, yield 90%). ^{1}H NMR (600 MHz, chloroform-d) δ 8.18(d, J=1.8 Hz, 1H), 8.16(d, J=1.6 Hz, 1H), 7.84(d, J=2.0 Hz, 1H), 7.83(d, J=2.1 Hz, 1H), 7.41(ddd, J=8.8, 7.2, 1.6 Hz, 2H), 7.29(d, J=2.1 Hz, 1H), 7.28-7.26(m, 3H), 6.63(s, 1H), 6.61(s, 1H).

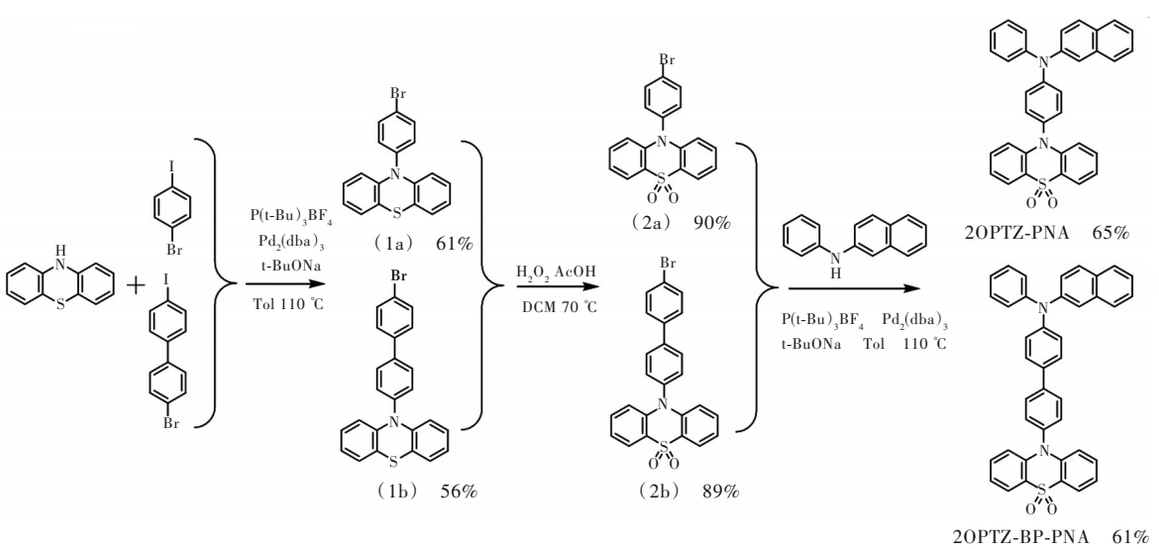

Fig.1 Chemical structures and synthetic routes of 2OPTZ-PNA and 2OPTZ-BP-PNA

Synthesis of 2OPTZ-PNA. The intermediate of 2a (1.16 g, 3.00 mmol), N-phenylnaphthalen-2-amine (0.72 g, 3.30 mmol), tri-tert-butylphosphine tetrafluoroborate (0.06 g, 0.2 mmol), sodium tert-butoxide (0.63 g, 6.6 mmol) were dissolved in toluene (50 mL) and the catalyst of tris(dibenzylideneacetone)dipalladium (0.09 g, 0.1 mmol) was added. The mixture solution was reacted at 110 ℃ for 8 h. When the reaction was over, the reaction solution was extracted, dried and column chromatography to give a white solid (1.02 g, yield 65%). ^{1}H NMR (600 MHz, chloroform-d): δ=8.18 (d, J=1.6 Hz, 1H), 8.16 (d, J=1.6 Hz, 1H), 7.84 (d, J=8.8 Hz, 1H), 7.82 (d, J=7.9 Hz, 1H), 7.70 (d, J=8.0 Hz, 1H), 7.61 (d, J= 2.3 Hz, 1H), 7.49-7.45 (m, 3H), 7.45-7.41 (m, 2H), 7.41-7.36 (m, 3H),

7.34-7.31 (m, 2H), 7.29 (dd, *J*=8.6, 1.1 Hz, 2H), 7.27-7.25 (dd, *J*=15.0, 0.9 Hz, 1H), 7.20-7.16 (m, 3H), 6.82(d, *J*=8.3 Hz, 2H). ^{13}C NMR (101 MHz, chloroform-d): δ=148.9, 147.0, 144.5, 141.1, 134.4, 132.8, 131.5, 131.0, 130.8, 129.8, 129.6, 127.7, 127.2, 126.6, 125.7, 125.3, 125.0, 124.5, 123.5, 123.4, 122.6, 122.4, 122.0, 117.4. HRMS (FAB/magnetic sector) *m/z*: $[M]^+$ calcd for $C_{34}H_{24}N_2O_2S$ 524.63; found 524.53.

2.1.2　2OPTZ-BP-PNA

Synthesis of 1b. It was prepared using a similar procedure to 1a. The obtained product was a white powder (2.41 g, yield 56%). ^{1}H NMR (600 MHz, chloroform-d): δ =7.76 (s, 2H), 7.63-7.59 (m, 2H), 7.55-7.52(m, 2H), 7.45(d, *J*=8.4 Hz, 2H), 7.05 (dd, *J*=7.5, 1.6 Hz, 2H), 6.95-6.75 (m, 4H), 6.32 (d, *J*=8.2 Hz, 2H).

Synthesis of 2b. It was prepared using a similar procedure to 2a. The obtained product was a white powder (1.41 g, yield 89%). ^{1}H NMR (600 MHz, chloroform-d) δ 8.19(dd, *J*=1.6, 0.5 Hz, 1H), 8.18 (dd, *J*=1.7, 0.5 Hz, 1H), 7.89-7.87(m, 1H), 7.87 (d, *J*=2.1 Hz, 1H), 7.67-7.64(m, 2H), 7.58-7.56 (m, 2H), 7.47(d, *J*=1.7 Hz, 1H), 7.46 (d, *J*=2.1 Hz, 1H), 7.41(ddd, *J*=8.7, 7.1, 1.6 Hz, 2H), 7.28-7.26(m, 2H), 6.71(d, *J*=8.7 Hz, 2H).

Synthesis of 2OPTZ-BP-PNA. It was prepared using a similar procedure to 2OPTZ-PNA. The resulting product is a white powder (1.10 g, yield 61%). ^{1}H NMR (600 MHz, DMSO-d6): δ=8.10(d, *J*=1.6 Hz, 1H), 8.09(d, *J*=1.6 Hz, 1H), 8.04(d, *J*=8.5 Hz, 2H), 7.91(d, *J*=8.9 Hz, 1H), 7.87(d, *J*=6.8 Hz, 1H), 7.79(d, *J*=8.7 Hz, 2H), 7.76(d, *J*=8.3 Hz, 1H), 7.60(ddd, *J*=8.8, 7.2, 1.7 Hz, 2H), 7.57(d, *J*=8.5 Hz, 2H), 7.53(d, *J*=2.3 Hz, 1H), 7.47-7.41 (m, 2H), 7.40-7.35 (m, 4H), 7.30 (dd, *J*=8.8, 2.3 Hz, 1H), 7.17(s, 1H), 7.17-7.15 (m, 3H), 7.14(d, *J*=7.4 Hz, 1H), 6.72(d, *J*=9.1 Hz, 2H). ^{13}C NMR (101 MHz, Chloroform-d): δ = 146.5, 146.5, 144.1, 143.2, 139.3, 138.7, 133.4, 133.0, 130.0, 129.2, 128.4, 128.0, 127.8, 126.8, 126.6, 126.0, 125.8, 125.7, 125.3, 123.7, 123.7, 123.6, 123.0, 122.3, 121.5, 119.8, 119.3, 115.2. HRMS (FAB/magnetic sector) *m/z*: $[M]^+$ calcd for $C_{40}H_{28}N_2O_2S$ 600.18; found 600.10.

2.2　Fabrication of OLEDs

The non-doped and doped OLEDs were fabricated by vacuum deposition. The glass substrates were cleaned with deionized water, acetone and ethanol. The electroluminescence (EL) spectra and CIE coordinates were measured by PR-655 spectrophotometer. The current density-voltage-luminance (*J-V-L*) characteristics were tested with the equipment of Keithley 2400 Source Meter and ST-900M Spot Brightness Meter. The characterization of devices was recorded at room temperature.

2.3　Characterizations

The Switzerland Bruker DR × 600 was used to measure the ^{1}H NMR and ^{13}C NMR spectra. Finnigan 4021C gas chromatography(GC)-mass spectrometry(MS) instrument was used to characterize mass spectra. Gaussian 09 program package with the B3LYP/6-31g (d) method was used to study theoretical calculations. The Lambda Bio 40, HORIBA FluoroMax-4 spectrophotometer and Edinburgh FLS 980 spectrometer were used to study the photophysical properties. Netzsch TG 209F3 and DSC Q2000 were used to investigate the TGA and DSC curves. CHI 660E electrochemical workstation was used to study cyclic voltammetry.

3　Results and Discussion

3.1　Theoretical Calculation

To further understand the relationship between the electronic structure and photophysical properties of 2OPTZ-PNA and 2OPTZ-BP-PNA, density functional theory (DFT) calculations were performed. The optimized molecular structures and the density state distributions of the LUMOs and the HOMOs were plotted in Fig. 2. From the optimized ground geometry, the dihedral angles of benzene ring and adjacent benzene ring, naphthalene group and benzene ring, phenothiazine oxide group and benzene ring of 2OPTZ-PNA were 68.13°, 66.82° and 86.25°. When the π-bridge length was extended to the biphenyl group, the corresponding dihedral angles became 68.94°, 67.25° and 87.16°, at the same time dihedral angle between the benzene rings on the biphenyl

group was 35.97°. It indicated that the elongation of π-conjugation did not change the twisted molecular configuration.

The HOMO of 2OPTZ-PNA was mainly distributed on the N-(2-naphthyl) aniline and the adjacent benzene ring, and its LUMO was mainly localized over the naphthylamine and adjacent benzene ring. By contrast, the HOMO distribution of 2OPTZ-BP-PNA was mainly on the N-(2-naphthyl) aniline and the biphenyl groups, and its LUMO was mainly localized over the naphthalene groups and adjacent biphenyl groups. In addition, it was found that both compounds had a significant degree of orbital overlap and separation between HOMO and LUMO, which may be led to a hybrid LE state and CT state. Furthermore, theoretically calculated band gaps of 2OPTZ-PNA and 2OPTZ-BP-PNA were 4.03 eV and 3.81 eV, respectively, guaranteeing emission in the violet-blue region. Fig. 2 (c) showed that prominent CT states were found, and 2OPTZ-BP-PNA had stronger oscillator strength (f=0.036 1) which is favorable to achieve higher PLQY.

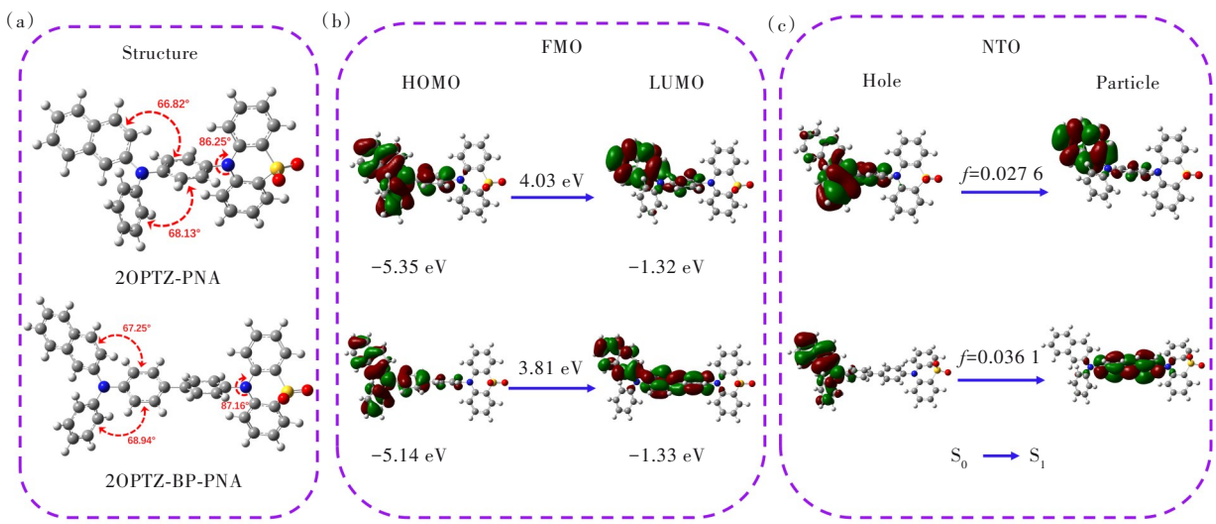

Fig.2 (a) The geometries and structural formulas of 2OPTZ-PNA and 2OPTZ-BP-PNA. (b) Spatial distribution of the HOMOs and LUMOs of 2OPTZ-PNA and 2OPTZ-BP-PNA. (c) The $S_0 \rightarrow S_1$ natural transition orbit (NTO) of 2OPTZ-PNA and 2OPTZ-BP-PNA.

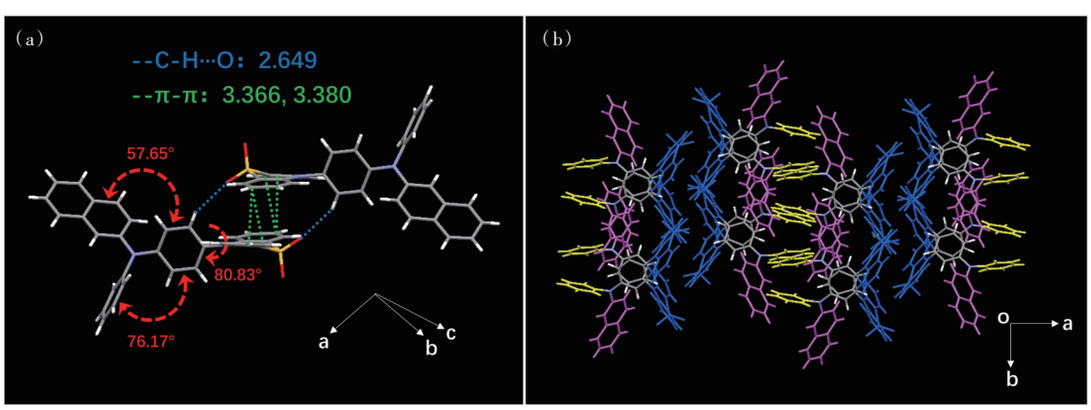

Fig.3 Inter-molecular interactions (a) and molecular packing structure (b) of the 2OPTZ-PNA crystal

3.2 Single-crystal Structure

Single crystal of 2OPTZ-PNA was obtained through slow diffusion of methyl alcohol into methylene dichloride. The crystal system of 2OPTZ-PNA was monoclinic, the space group was $P21/c$, and there were four molecules in one unit cell (Tab. S1). As shown in Fig. 3(a), the twisted dihedral angle between the benzene ring and the central benzene ring, the naphthalene group and central benzene ring, the phenothiazine oxide group and central benzene

ring of 2OPTZ-PNA are 76.17°, 57.65° and 80.83°, which is a small difference from the dihedral angle from theoretical calculations. There is strong intermolecular interaction of π-π stacking (0.336 nm and 0.338 0 nm) between phenothiazine oxide groups in adjacent molecules. Moreover, typical C—H···O hydrogen bonds (0.264 9 nm) between the oxygen atom and the central benzene groups were found. It indicated that more planar molecular structure in the single crystal resulted from the stronger π-π stacking and hydrogen bonds. Fig. 3(b) showed that the molecular stacking owned the head-to-head arrangements.

3.3 Photophysical Properties

Photophysical properties of 2OPTZ-PNA and 2OPTZ-BP-PNA were measured in 10^{-5} mol/L toluene solution (Fig. 4(a)) and vacuum-deposited neat films (Fig. 4(b)). From the absorption spectra in the toluene solution, absorption bands of both compounds between 300 nm and 340 nm were assigned as π-π* transition[41-42] and the long-wavelength absorption peaks between 370 nm and 400 nm, respectively, were attributed to the intramolecular charge transfer state. Photoluminescence(PL) emission peaks in toluene solution of 2OPTZ-PNA and 2OPTZ-BP-PNA were located at 391/500 nm and 402 nm, respectively. In the neat films, PL emission peaks of 2OPTZ-PNA and 2OPTZ-BP-PNA were at 411 nm and 429 nm belong to the violet-blue light, respectively, which had a red-shift of about 20 nm and 27 nm owing to the aggregate state. By comparison, 2OPTZ-BP-PNA had an obvious red shift than 2OPTZ-PNA because of the change of electronic structure by the extended π-bridge. Additionally, the absolute PLQY values (14% and 33%) and their lifetime (3.20 ns and 2.47 ns, Fig. S4) of 2OPZT-PNA and 2OPTZ-BP-PNA were obtained in the neat films. It indicated that the expansion of π-bridge could effectively enhance the PLQY values by adjusting the CT state that has stronger oscillator strength.

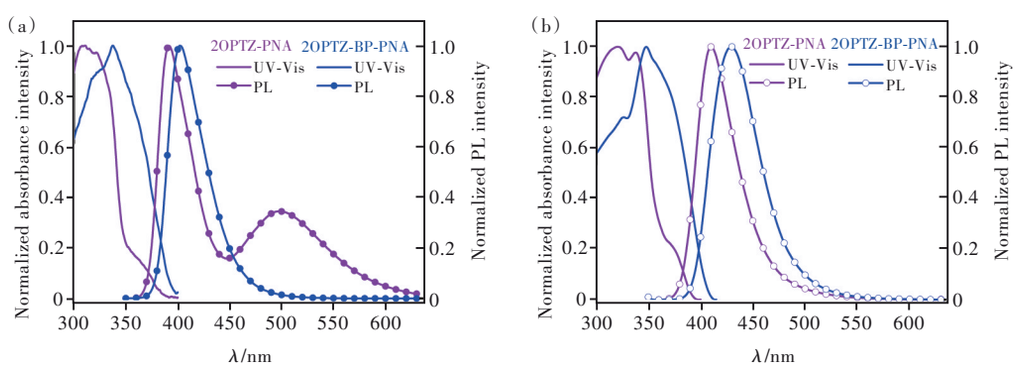

Fig.4　The UV-Vis absorption spectra and PL spectra of 2OPTZ-PNA and 2OPTZ-BP-PNA in toluene solution (10^{-5} mol/L) (a) and in the neat film (b)

In order to further investigate the photophysical properties, we measured the UV-Vis absorption spectra (Fig. S5), PL spectra and time-dependent fluorescence spectroscopy (Fig. 5) of 2OPTZ-PNA and 2OPTZ-BP-PNA in different polar solvents. UV absorption bands of both compounds had no significant changes in the different solvents, indicating that their electron transition in the absorption process was similar. However, PL emission of 2OPTZ-PNA and 2OPTZ-BP-PNA exhibited a remarkable solvatochromic effect. As shown in Fig. 5(a), emission peaks of 2OPTZ-PNA showed obvious red-shift from low-polarity n-hexane to high-polarity dimethyl sulfoxide (DMSO) and extra PL emission band presented at the long-wavelength region. It could be explained as that HOMO and LUMO of 2OPTZ-PNA were located at triarylamine groups leading to the hybrid emission from the locally excited states(LE) state and CT state. However, the emission peak of 2OPTZ-BP-PNA exhibited a red shift of 50 nm in the different solvents, which was attributed to the obvious CT characteristics. We used the Lippert-Mataga model[43] to estimate the excited state dipole moments with increasing the solvent polarities. Both

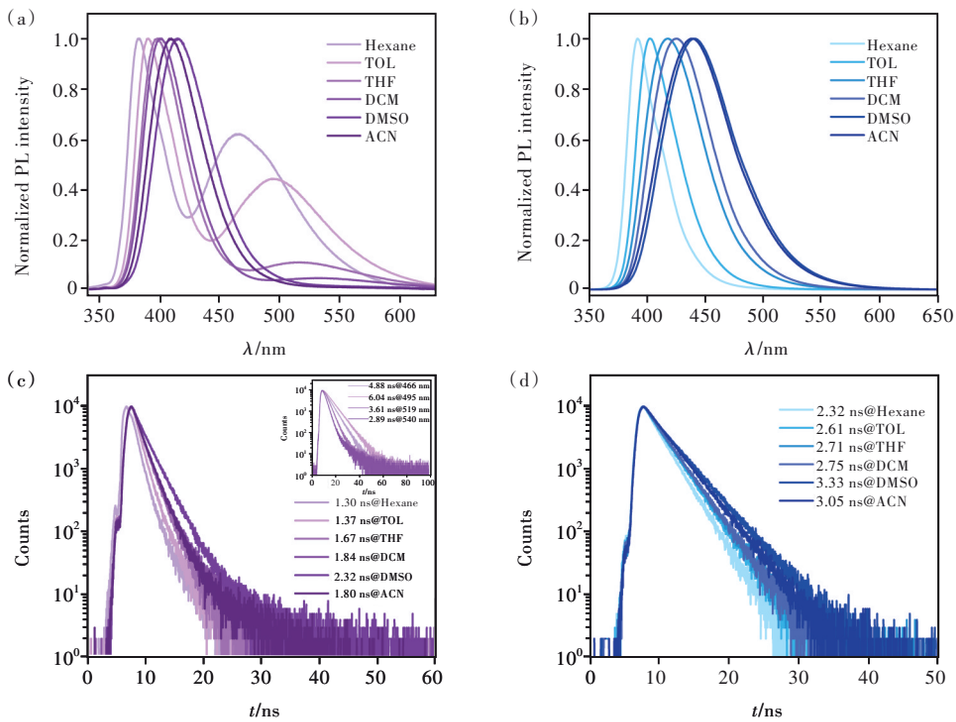

Fig.5 Photophysical properties in different solvents. PL spectra of 2OPTZ-PNA (a) and 2OPTZ-BP-PNA (b). Time-dependent fluorescence spectra of 2OPTZ-PNA (c) and 2OPTZ-BP-PNA (d). Inset: time-dependent fluorescence spectra of 2OPTZ-PNA measured at 466, 495, 519, 540 nm.

compounds exhibited a linear relationship (Fig. S6) and their excited dipole moment (μ_e) values of 2OPTZ-PNA and 2OPTZ-BP-PNA were 18.79 D and 22.06 D, respectively. In addition, PL decay lifetime of 2OPTZ-PNA in different solvents ranged from 1.30 ns to 2.32 ns, while 2OPTZ-BP-PNA had a longer lifetime from 2.32 ns to 3.33 ns. The above results testified that the extension of π-bridge could optimize the intramolecular charge transfer (ICT) states.

3.4 Thermal and Electrochemical Properties

Thermal properties of 2OPTZ-PNA and 2OPTZ-BP-PNA were investigated by thermalgravimetric analysis (TGA) and differential scanning calorimetry (DSC) under nitrogen atmosphere(Fig. 6(a) and Tab. 1). It showed that 2OPTZ-PNA and 2OPTZ-BP-PNA possessed good thermal and morphological stabilities with the high decomposition temperatures (T_d, corresponding to 5% weight loss) of 370/447 ℃ and glass-transition temperatures(T_g) of 106/134 ℃, respectively. It indicated that both compounds were suitable to fabricate the stable OLEDs by vacuum thermal evaporation. It was worth mentioning that 2OPTZ-BP-PNA had more excellent thermal stability owing to the rigidly molecular structure by the extended π-bridge length.

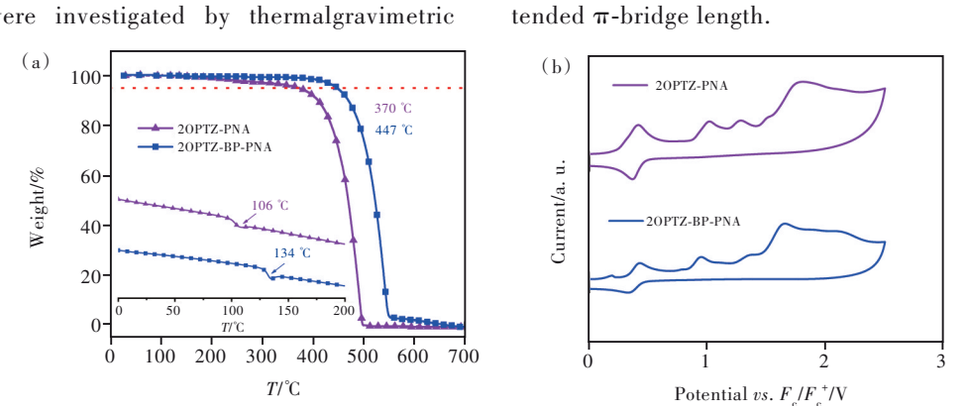

Fig.6 TGA and DSC curves (inset)(a) and electrochemical CV curves(b) of 2OPTZ-PNA and 2OPTZ-BP-PNA

Tab. 1　The thermal properties and photophysical data of 2OPTZ-PNA and 2OPTZ-BP-PNA

Compounds	λ_{abs}[a]/nm	λ_{em}[a]/nm	λ_{em}[b]/nm	λ_{em}[c]/nm	HOMO/LUMO/eV	Φ_{PL}[b]/ %	T_d /T_g/℃
2OPTZ-PNA	310, 370	391, 500	411	439	−5.40/−1.93	14	370/106
2OPTZ-BP-PNA	320, 337	402	429	424	−5.32/−2.12	33	447/134

[a] Measured in toluene solution (10^{-5} mol/L). [b] Measured in the neat film. [c] Measured in powder.

Electrochemical properties of 2OPTZ-PNA and 2OPTZ-BP-PNA were evaluated by cyclic voltammetry (CV) curves (Fig. 6(b)), which were used to calculate the HOMO and LUMO energy levels. According to the formula of $E_{HOMO}=-4.8-e(E_e^{ox}-E_f^{ox})$, the HOMO energy levels of 2OPTZ-PNA and 2OPTZ-BP-PNA were −5.40 eV and −5.32 eV, respectively, which were calculated from the oxidation potential with ferrocene as an internal reference. Correspondingly, the LUMO energy levels calculated from the formula of $E_{LUMO}=E_{HOMO}+E_g$ were −1.93 eV and −2.12 eV, respectively.

3.5　Film Morphology Characteristic

As is well-known that the excellent film morphologies for the light-emitting layer are favor to reduce the interface problems and improve device efficiency. On this basis, film morphologies of both compounds in the thermally evaporated thin film were evaluated by atomic force microscopy (AFM). As shown in Fig. 7, the root mean square surface roughness values of 2OPTZ-PNA and 2OPTZ-BP-PNA are 0.36 nm and 0.24 nm, respectively. It indicated that 2OPTZ-BP-PNA would have better contact with the adjacent functional layers owing to the smoother and more homogeneous surface morphology.

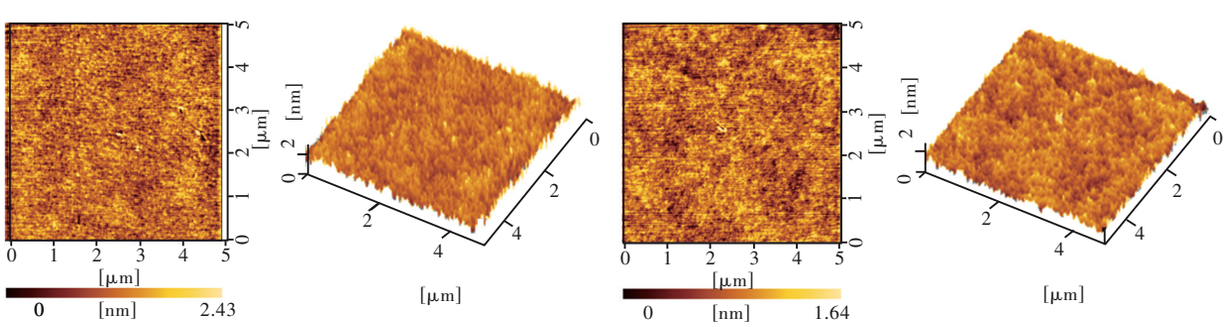

2OPTZ-PNA　RMS=0.36 nm　2OPTZ-BP-PNA　RMS=0.24 nm

Fig.7　AFM images (5 μm × 5 μm) and the corresponding 3D height images of 2OPTZ-PNA and 2OPTZ-BP-PNA in the evaporated films

3.6　Electroluminescent Performance

In order to evaluate the EL performance of 2OPTZ-PNA and 2OPTZ-BP-PNA, non-doped devices were firstly fabricated. The device structures were as follows: ITO/MoO_3 (3 nm)/NPB (40 nm)/TCTA (10 nm)/2OPTZ-PNA or 2OPTZ-BP-PNA (20 nm)/TPBi (40 nm)/LiF (1 nm)/Al (100 nm). The molecular structures of related functional layer materials, device structures and energy-level diagrams are shown in Fig. S8. Fig. 8 showed the EL properties of these non-doped devices, and the critical data were summarized in Tab. 2. Both 2OPTZ-PNA-based and 2OPTZ-BP-PNA-based non-doped devices achieved violet-blue emission, and their emission peaks were located at 424 nm and 436 nm with the corresponding CIE coordinates at (0.164, 0.060) and (0.155, 0.046), respectively. Here, apart from the slight red shift of EL emissions, EL spectra for two devices were similar to the PL spectra in the neat films prepared by vacuum-deposition, indicating that EL emissions for these devices were well originated from the intrinsic emission of two materials.

Moreover, EL spectra of 2OPTZ-PNA and 2OPTZ-BP-PNA at different driving voltages exhibited good color stability without noticeable changes (Fig. S9). The lower turn-on voltages (3.0−3.2 V) were obtained, which could be attributed to the use of a suitable device structure and the balanced carrier

transport properties characterized by the carrier-only devices (Fig. S10). In particular, the non-doped 2OPTZ-BP-PNA-based device exhibited excellent EL performance with the maximum EQE and luminance (L_{max}) of 4.1% and 2 602 cd/m^2, respectively. Importantly, it also had the narrower FWHM of 54 nm, and CIE coordinates of (0.155, 0.046) at the driving voltage of 6 V was very close to the standard violet-blue light in the high-definition displays. The high EQE of 2OPTZ-BP-PNA was due to its better carrier transport performance, more suitable device energy levels and high PLQY.

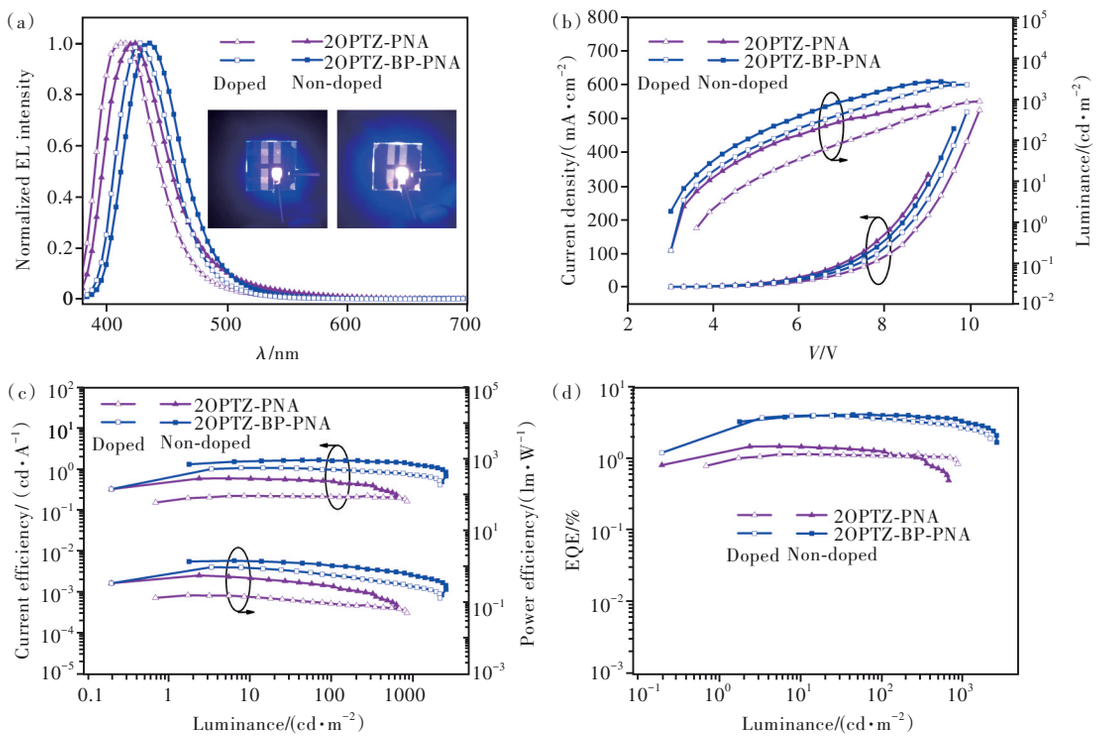

Fig.8 (a) EL performance of 2OPTZ-PNA and 2OPTZ-BP-PNA in the non-doped and doped devices. EL spectra at a driving voltage of 5 V. (b) *J*-*V*-*L* curves. (c) CE-*L*-PE curves. (d) EQE-*L* curves.

Tab. 2 EL performance of devices based on 2OPTZ-PNA and 2OPTZ-BP-PNA

Devices	λ_{EL}/nm	V_{on}[a]/V	L_{max}/(cd·m^{-2})	CE_{max}/(cd·A^{-1})	PE_{max}/(lm·W^{-1})	EQE_{max}/%	CIE (x, y)	FWHMs/nm
2OPTZ-PNA	424	3.2	666	0.60	0.57	1.5	(0.164, 0.060)	57
mCP:2OPTZ-PNA	414	3.7	861	0.23	0.16	1.1	(0.162, 0.036)	54
2OPTZ-BP-PNA	436	3.0	2602	1.67	1.46	4.1	(0.155, 0.046)	54
mCP:2OPTZ-BP-PNA	428	3.2	2180	1.09	0.96	3.9	(0.157, 0.034)	51

[a] Turn-on voltage estimated at a brightness of 1 cd/m^2.

Furthermore, we also tried to explore the EL properties of 2OPTZ-PNA and 2OPTZ-BP-PNA in the doped devices, where mCP was employed as the host material of 2OPTZ-PNA and 2OPTZ-BP-PNA. The device structure was ITO/MoO_3(3 nm)/NPB(40 nm)/TCTA(10 nm)/mCP:x% 2OPTZ-PNA or 2OPTZ-BP-PNA (20 nm)/TPBi(40 nm)/LiF(1 nm)/Al (100 nm). Compared with their non-doped devices, the EL emission spectra of two doped devices had significantly blue-shifted emission peaks and narrower FWHMs(Fig. 8 and Tab. 2). This was mainly attributed to the fact that the introduction of the host material (mCP) reduced the polarity of the emitting layer and weakened the intermolecular interaction. Moreover, we investigated the different doping concentrations of 70%, 50%, 30%, 20% and 10% in the doped 2OPTZ-BP-PNA-based devices (Fig. S11-S12). As the doping concentration decreased (Tab. S2), EL

emission peaks had obvious blue-shift to a certain extent owing to increasing the distance between the chromophores. When the doping concentration was 70%, it showed high-quality violet-blue light emission at 428 nm with a CIE coordinate of (0.156, 0.036). However, the maximum luminance and device efficiency were slightly lower than the non-doped device. It could be explained that the disordered molecular arrangement in the doped films decreased the light output. These results indicated that the new compounds of 2OPTZ-PNA and 2OPTZ-BP-PNA had great potential in lighting and full-color display.

4 Conclusion

In summary, we have designed and synthesized a kind of violet-blue fluorescent materials (2OPTZ-PNA and 2OPTZ-BP-PNA) with D-π-A-typed structures using 10H-phenothiazine 5, 5-dioxide as the weak acceptor and N-(2-naphthyl) aniline as the donor and the phenyl and biphenyl as the π-bridge. By prolonging the π-bridge length, the charge transfer state has been appropriately regulated and controlled. On this basis, PLQYs improved from 14% to 33%. Non-doped OLED devices based on 2OPTZ-PNA and 2OPTZ-BP-PNA exhibited purely violet-blue light with the CIE coordinates of (0.164, 0.060) and (0.155, 0.046), respectively. Furthermore, the non-doped devices of 2OPTZ-BP-PNA exhibited the best EL performance with the narrow FWHM of 54 nm and maximum EQEs of 4.1%. This work provides a new strategy for high-performance violet-blue emitters.

Supplementary Information and Response Letter are available for this paper at: http://cjl.lightpublishing.cn/thesisDetails#10.37188/CJL.20220093.

References:

[1] LIN C W, HAN P B, XIAO S, *et al.* Efficiency breakthrough of fluorescence OLEDs by the strategic management of "hot excitons" at highly lying excitation triplet energy levels [J]. *Adv. Funct. Mater.*, 2021, 31(48): 2106912-1-8.

[2] XU R P, LI Y Q, TANG J X. Recent advances in flexible organic light-emitting diodes [J]. *J. Mater. Chem.* C, 2016, 4(39): 9116-9142.

[3] YANG Z Y, MAO Z, XIE Z L, *et al.* Recent advances in organic thermally activated delayed fluorescence materials [J]. *Chem. Soc. Rev.*, 2017, 46(3): 915-1016.

[4] GUO X M, YUAN P S, FAN J Z, *et al.* Unraveling the important role of high-lying triplet-lowest excited singlet transitions in achieving highly efficient deep-blue AIE-based OLEDs [J]. *Adv. Mater.*, 2021, 33(11): 2006953-1-8.

[5] 贾钧森, 王飞, 赵波, 等. D-π-A-π-D型小分子红光材料的制备及其性能 [J]. 发光学报, 2020, 41(1): 9-15.
JIA J S, WANG F, ZHAO B, *et al.* Design, synthesis and properties of D-π-A-π-D type organic red light luminogens [J]. *Chin. J. Lumin.*, 2020, 41(1): 9-15. (in Chinese)

[6] ZHANG Y M, WANG Y F, SONG J, *et al.* Near-infrared emitting materials *via* harvesting triplet excitons: molecular design, properties, and application in organic light emitting diodes [J]. *Adv. Opt. Mater.*, 2018, 6(18): 1800466-1-19.

[7] CHEN W C, YUAN Y, NI S F, *et al.* Achieving efficient violet-blue electroluminescence with CIE_y <0.06 and EQE>6% from naphthyl-linked phenanthroimidazole-carbazole hybrid fluorophores [J]. *Chem. Sci.*, 2017, 8(5): 3599-3608.

[8] CHEN Z, LIU X K, ZHENG C J, *et al.* High performance exciplex-based fluorescence-phosphorescence white organic light-emitting device with highly simplified structure [J]. *Chem. Mater.*, 2015, 27(15): 5206-5211.

[9] CHOU H H, CHEN Y H, HSU H P, *et al.* Synthesis of diimidazolylstilbenes as n-type blue fluorophores: alternative dopant materials for highly efficient electroluminescent devices [J]. *Adv. Mater.*, 2012, 24(43): 5867-5871.

[10] SUN J, JIA J S, ZHAO B, *et al.* A purely organic D-π-A-π-D emitter with thermally activated delayed fluorescence and room temperature phosphorescence for near-white OLED [J]. *Chin. Chem. Lett.*, 2021, 32(4): 1367-1371.

[11] CHEN W C, WU G F, YUAN Y, *et al.* A *meta*-molecular tailoring strategy towards an efficient violet-blue organic electroluminescent material [J]. *RSC Adv.*, 2015, 5(23): 18067-18074.

[12] SHINAR J, SHINAR R. Organic light-emitting devices (OLEDs) and OLED-based chemical and biological sensors: an overview [J]. *J. Phys.* D: *Appl. Phys.*, 2008, 41(13): 133001-1-26.

[13] TONGE C M, ZENG J J, ZHAO Z J, *et al*. Bis (hexamethylazatriangulene)sulfone: a high-stability deep blue-violet fluorophore with 100% quantum yield and CIE_y < 0.07 [J]. *J. Mater. Chem.* C, 2020, 8(15): 5150-5155.

[14] GAO Z, LIU Y L, WANG Z M, *et al*. High-efficiency violet-light-emitting materials based on phenanthro[9, 10-*d*]imidazole [J]. *Chem. Eur. J.*, 2013, 19(8): 2602-2605.

[15] THAKARE D S, OMANWAR S K, MUTHAL P L, *et al*. UV-emitting phosphors: synthesis, photoluminescence and applications [J]. *Phys. Status Solidi* A, 2004, 201(3): 574-581.

[16] LY K T, CHEN-CHENG R W, LIN H W, *et al*. Near-infrared organic light-emitting diodes with very high external quantum efficiency and radiance [J]. *Nat. Photonics*, 2017, 11(1): 63-68.

[17] IM Y, BYUN S Y, KIM J H, *et al*. Recent progress in high-efficiency blue-light-emitting materials for organic light-emitting diodes [J]. *Adv. Funct. Mater.*, 2017, 27(13): 1603007-1-24.

[18] WANG Z Q, YANG T T, DONG S F, *et al*. Anthracene and carbazole based asymmetric fluorescent materials for high-efficiency deep-blue non-doped organic light emitting devices with CIE_y=0.06 [J]. *Dyes Pigments*, 2022, 199: 110047.

[19] WANG S M, ZHANG H Y, ZHANG B H, *et al*. Towards high-power-efficiency solution-processed OLEDs: material and device perspectives [J]. *Mater. Sci. Eng.: R: Rep.*, 2020, 140: 100547-1-61.

[20] HAN P B, LIN C W, MA D G, *et al*. Violet-blue emitters featuring aggregation-enhanced emission characteristics for nondoped OLEDs with CIE_y smaller than 0.046 [J]. *ACS Appl. Mater. Interfaces*, 2020, 12(41): 46366-46372.

[21] XIA G Q, QU C, ZHU Y L, *et al*. A TADF emitter featuring linearly arranged spiro-donor and spiro-acceptor groups: efficient nondoped and doped deep-blue OLEDs with CIE_y <0.1 [J]. *Angew. Chem. Int. Ed.*, 2021, 60(17): 9598-9603.

[22] 卢国婧, 廖小青, 李璐, 等. 基于扭曲 A-π-D-π-A 构型的蓝色荧光材料的 π-共轭桥与光物理特性间的关系 [J]. 发光学报, 2019, 40(11): 1334-1347.
LU G J, LIAO X Q, LI L, *et al*. Relationship between π-conjugated bridge and photophysical properties of blue light-emitting fluorescent materials with twisting A-π-D-π-A configuration [J]. *Chin. J. Lumin.*, 2019, 40(11): 1334-1347. (in English)

[23] HAN C M, ZHAO F C, ZHANG Z, *et al*. Constructing low-triplet-energy hosts for highly efficient blue PHOLEDs: controlling charge and exciton capture in doping systems [J]. *Chem. Mater.*, 2013, 25(24): 4966-4976.

[24] FISHER A L, LINTON K E, KAMTEKAR K T, *et al*. Efficient deep-blue electroluminescence from an ambipolar fluorescent emitter in a single-active-layer device [J]. *Chem. Mater.*, 2011, 23(7): 1640-1642.

[25] RAJAMALLI P, CHEN D Y, SURESH S M, *et al*. Planar and rigid pyrazine-based TADF emitter for deep blue bright organic light-emitting diodes [J]. *Eur. J. Org. Chem.*, 2021, 2021(16): 2285-2293.

[26] ZHANG J, YE H R, JIN Y X, *et al*. Recent progress in near-infrared organic electroluminescent materials [J]. *Top. Curr. Chem.*, 2022, 380(1): 6-1-40.

[27] OUYANG X H, LI X L, ZHANG X Y, *et al*. Effective management of intramolecular charge transfer to obtain from blue to violet-blue OLEDs based on a couple of phenanthrene isomers [J]. *Dyes Pigments*, 2015, 122: 264-271.

[28] LI Z Q, LI C L, XU Y C, *et al*. Nonsymmetrical connection of two identical building blocks: constructing donor-acceptor molecules as deep blue emitting materials for efficient organic emitting diodes [J]. *J. Phys. Chem. Lett.*, 2019, 10(4): 842-847.

[29] CHEN S, ZHANG C Y, XU H. Achieving host-free near-ultraviolet electroluminescence *via* electronic state engineering with phosphine oxide [J]. *Chem. Eng. J.*, 2022, 429: 132327.

[30] SHI J J, XU L, CHEN C, *et al*. Efficient and color-purity blue electroluminescence by manipulating the coupling forms of D-A hybrids with phenothiazine as the strong donor [J]. *Dyes Pigments*, 2019, 160: 962-970.

[31] CHEN Z, HO C L, WANG L Q, *et al*. Single-molecular white-light emitters and their potential WOLED applications [J]. *Adv. Mater.*, 2020, 32(11): 1903269-1-45.

[32] WEI J B, LIANG B Y, DUAN R H, *et al*. Induction of strong long-lived room-temperature phosphorescence of N-Phenyl-2-naphthylamine molecules by confinement in a crystalline dibromobiphenyl matrix [J]. *Angew. Chem. Int. Ed.*, 2016, 55(50): 15589-15593.

[33] XIANG S P, HUANG Z, SUN S Q, *et al*. Highly efficient non-doped OLEDs using aggregation-induced delayed fluorescence materials based on 10-phenyl-10*H*-phenothiazine 5, 5-dioxide derivatives [J]. *J. Mater. Chem.* C, 2018, 6(42): 11436-11443.

[34] ROUT Y, MONTANARI C, PASCIUCCO E, *et al.* Tuning the fluorescence and the intramolecular charge transfer of phenothiazine dipolar and quadrupolar derivatives by oxygen functionalization [J]. *J. Am. Chem. Soc.*, 2021, 143(26): 9933-9943.

[35] YAO L, SUN S H, XUE S F, *et al.* Aromatic S-heterocycle and fluorene derivatives as solution-processed blue fluorescent emitters: structure-property relationships for different sulfur oxidation states [J]. *J. Phys. Chem.* C, 2013, 117(27): 14189-14196.

[36] GAO Y, ZHANG S T, PAN Y Y, *et al.* Hybridization and de-hybridization between the locally-excited (LE) state and the charge-transfer (CT) state: a combined experimental and theoretical study [J]. *Phys. Chem. Chem. Phys.*, 2016, 18(35): 24176-24184.

[37] HOU M N, WANG H, MIAO Y Q, *et al.* Highly efficient deep-blue electroluminescence from a A-π-D-π-A structure based fluoresence material with exciton utilizing efficiency above 25% [J]. *ACS Appl. Energy Mater.*, 2018, 1(7): 3243-3254.

[38] LI Y C, LI X L, CAI X Y, *et al.* Deep blue fluorophores incorporating sulfone-locked triphenylamine: the key for highly efficient fluorescence-phosphorescence hybrid white OLEDs with simplified structure [J]. *J. Mater. Chem.* C, 2015, 3(27): 6986-6996.

[39] SHOER L E, EATON S W, MARGULIES E A, *et al.* Photoinduced electron transfer in 2,5,8,11-tetrakis-donor-substituted Perylene-3,4:9,10-bis (dicarboximides) [J]. *J. Phys. Chem.* B, 2015, 119(24): 7635-7643.

[40] YU M X, ZHU X Y, ZENG J J, *et al.* Comparative study on the impact of through-space charge transfer over the electroluminescence performance of delayed fluorescence molecules [J]. *J. Mater. Chem.* C, 2021, 9(41): 14808-14814.

[41] ZHANG Y, LAI S L, TONG Q X, *et al.* High efficiency nondoped deep-blue organic light emitting devices based on imidazole-π-triphenylamine derivatives [J]. *Chem. Mater.*, 2012, 24(1): 61-70.

[42] TANG X Y, SHAN T, BAI Q, *et al.* Efficient deep-blue electroluminescence based on phenanthroimidazole-dibenzothiophene derivatives with different oxidation states of the sulfur atom [J]. *Chem. Asian J.*, 2017, 12(5): 552-560.

[43] DU C Y, LIU F T, LIU H, *et al.* Non-doped organic light-emitting diodes based on phenanthroimidazole-triphenylamine derivatives with a low efficiency roll-off of 9% at a high luminance of 10 000 $cd \cdot m^{-2}$ [J]. *J. Mater. Chem.* C, 2020, 8(41): 14446-14452.

崔江峰(1995-),男,河北沧州人,硕士研究生,2018年于河北科技大学获得学士学位,主要从事有机光电材料与器件的研究。
E-mail: 1689813420@qq.com

王华(1977-),男,山西平定人,博士,教授,博士生导师,2007年于太原理工大学获得博士学位,主要从事有机半导体光电材料与器件的研究
E-mail: wanghua001@tyut.edu.cn

孙静(1987-),女,山东潍坊人,博士,讲师,2016年于太原理工大学获得博士学位,主要从事有机光电功能材料的研究。
E-mail: sunjing@tyut.edu.cn